Excitation of superconducting qubits from hot non-equilibrium quasiparticles

J. Wenner[1], Yi Yin[1],* Erik Lucero[1],† R. Barends[1], Yu Chen[1], B. Chiaro[1], J. Kelly[1], M. Lenander[1], Matteo Mariantoni[1,2], A. Megrant[1,3], C. Neill[1], P. J. J. O'Malley[1], D. Sank[1], A. Vainsencher[1], H. Wang[1,4], T. C. White[1], A. N. Cleland[1,2], and John M. Martinis[1,2‡]

[1]*Department of Physics, University of California, Santa Barbara, CA 93106, USA*
[2]*California NanoSystems Institute, University of California, Santa Barbara, CA 93106, USA*
[3]*Department of Materials, University of California, Santa Barbara, CA 93106, USA and*
[4]*Department of Physics, Zhejiang University, Hangzhou 310027, China*

Superconducting qubits probe environmental defects such as non-equilibrium quasiparticles, an important source of decoherence. We show that "hot" non-equilibrium quasiparticles, with energies above the superconducting gap, affect qubits differently from quasiparticles at the gap, implying qubits can probe the dynamic quasiparticle energy distribution. For hot quasiparticles, we predict a non-neligable increase in the qubit excited state probability P_e. By injecting hot quasiparticles into a qubit, we experimentally measure an increase of P_e in semi-quantitative agreement with the model.

PACS numbers: 74.50.+r, 03.65.Yz, 85.25.Cp, 74.25.F-, 03.67.Lx

The superconducting qubit [1, 2] is an excellent candidate for building a quantum computer, as demonstrated by recent implementations of the Toffoli gate [3, 4] along with simple forms of quantum error correction [5] and Shor's algorithm [6]. However, qubit performance is affected by interactions with a range of environmental defects, including individual two-level states [7, 8] and flux noise [9–11]. As such, superconducting qubits are a sensitive probe of the physics of microscopic defects. Non-equilibrium quasiparticles present another important class of defects, which have recently been shown to cause qubit decoherence [12–18]. The sensitivity of qubits to quasiparticles, and their ability to measure both energy emission and absorption rates, enables new measurements of the non-equilibrium properties of superconductors.

In several recent experiments, the excited state populations of superconducting qubits were measured to be in excess of thermal equilibrium values, an effect attributed to thermal heating induced by non-equilibrium quasiparticles [18–21]. This was supported by the observation that the qubit excited-state population was significantly lowered when the level of stray infrared radiation, and hence quasiparticle density [22], was reduced [18]. In these experiments, the quasiparticle-induced thermal heating necessary to produce the excited state population was thought to result in effective qubit temperatures of 70-200 mK [18–20, 23], even though these temperatures are comparable to the qubit energy $E_{ge} \sim 300$ mK. This violates the typical assumption [15, 22, 24, 25] that $(E-\Delta), k_BT \ll E_{ge}$ for characteristic quasiparticle energies E, superconducting gap Δ, and dilution refrigerator temperature $T \simeq 20$ mK. This means that the specifics of the quasiparticle energy distribution cannot be neglected.

Here, we provide a quantitative theory explaining how "hot" quasiparticles can directly excite qubits, providing a model for these and other experiments which have measured qubits with non-negligible excited state populations [23, 26–29] and excitation rates [19]. We further provide an experimental test of this model by injecting a non-equilibrium quasiparticle population into a superconducting qubit and using the qubit to dynamically probe this population. We find semi-quantitative agreement between our model and the experimental data presented here, showing that non-equilibrium quasiparticles provide a mechanism for the spurious excitation of superconducting qubits, distinct from thermal effects. In addition, our approach provides a new method to study the temporal dynamics of the non-equilibrium quasiparticle energy distribution and can be used to validate alternative methods [30].

A quasiparticle tunneling through the Josephson junction barrier in a qubit can cause both excitation and dissipation in the qubit, as illustrated in Fig. 1. Consider a qubit initially in its excited state: A "cold" quasiparticle near the gap energy can absorb the qubit transition energy E_{ge} between the qubit's excited $|e\rangle$ and its ground $|g\rangle$ states, causing the qubit to switch to its ground state (blue arrows in Fig. 1(a) and (b)). Any quasiparticle in the junction area can absorb this energy, so the qubit $|e\rangle \rightarrow |g\rangle$ decay rate $\Gamma_\downarrow$ due to this channel is proportional to the quasiparticle density n_{qp}. For a qubit initially in its ground state, a "hot" quasiparticle sufficiently above the gap energy can excite the qubit, but only if the quasiparticle has energy greater than $\Delta + E_{ge}$ (red arrows in Fig. 1(a) and (c)). The qubit $|g\rangle \rightarrow |e\rangle$ excitation rate $\Gamma_\uparrow$ thus depends on the energy distribution of the quasiparticle population.

If the quasiparticle population were well-described by a temperature $T \simeq 20\,\text{mK} \ll E_{ge}/k_B$, then a negligible qubit excitation rate $\Gamma_\uparrow$ would be expected, as in Fig. 1(b). There are however a number of processes that can produce quasiparticles with energies well above k_BT, which then relax via quasiparticle-phonon scattering [31],

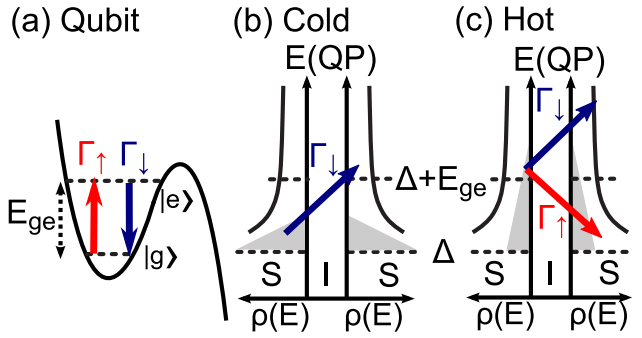

FIG. 1: (Color online) Qubit decay $\Gamma_\downarrow$ (blue) and excitation $\Gamma_\uparrow$ (red) mediated by tunneling quasiparticles. (a) Portion of the superconducting phase qubit potential energy diagram, showing the $\Gamma_\downarrow$ and $\Gamma_\uparrow$ transitions between the ground state $|g\rangle$ and the excited state $|e\rangle$, along with the qubit energy E_{ge}. (b) Cold non-equilibrium quasiparticles, which have energies near the superconducting gap Δ, can only absorb E_{ge}, resulting in qubit $\Gamma_\downarrow$ decay. The density of states ($\rho(E)$, horizontal) on both sides of a Josephson junction (superconductor S - insulator I - superconductor S) is shown versus quasiparticle energy E (vertical). The quasiparticle energy distribution $f(E)$ is shown by the shaded triangles. (c) Hot non-equilibrium quasiparticles with energy above $\Delta + E_{ge}$ (portion of $f(E)$ with $E > \Delta + E_{ge}$) not only can cause qubit $\Gamma_\downarrow$ transitions but can also relax by causing qubit $|g\rangle \rightarrow |e\rangle$ transitions.

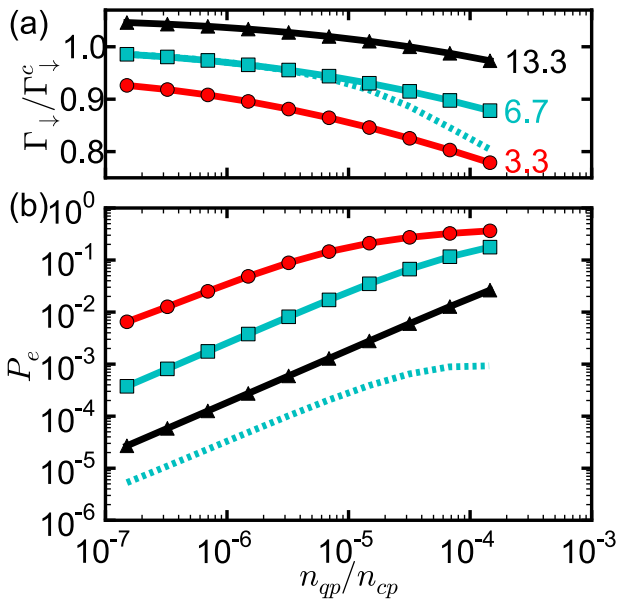

FIG. 2: (Color online) Calculated effects of hot quasiparticles. Quasiparticle densities incorporate scattering and recombination, with quasiparticles injected at energy $E_{inj} = 1.8\Delta$ (solid lines) or $\Delta + 0.94E_{ge}$ (dashed line), assuming $\Delta/k_B = 2\,\mathrm{K}$ as for aluminum. Plots are for three different qubit frequencies E_{ge}/h: 13.3 GHz (black), 6.7 GHz (green), and 3.3 GHz (red); lines are guides to the eye. (a) Qubit decay rate $\Gamma_\downarrow$ normalized by the cold rate $\Gamma_\downarrow^c$ from Eq. (2), showing that $\Gamma_\downarrow^c$ is a good approximation to $\Gamma_\downarrow$. (b) Qubit $|e\rangle$ state probability $P_e = \Gamma_\uparrow/(\Gamma_\downarrow + \Gamma_\uparrow)$ vs. normalized quasiparticle density n_{qp}/n_{cp}. The $|e\rangle$ state occupation increases linearly with the quasiparticle density for low densities. Injecting low energy quasiparticles (dashed line) results in a greatly reduced P_e.

but for which the non-equilibrium quasiparticle occupation probability $f(E)$ still has a significant population of hot quasiparticles[13], with energies well above k_BT. The distribution $f(E)$ is typically not thermal.

In order to model the steady-state quasiparticle distribution, we assume quasiparticles are injected in the junction at a constant rate at an energy E_{inj} well above $\Delta + E_{ge}$, with the resulting quasiparticle density n_{qp} scaling as the square root of the injection rate; we verify below (Fig. 3) that the qubit excited state probability P_e is independent of the injection energy. Steady state is achieved by balancing phonon scattering and quasiparticle injection and recombination[32]. Although the resulting steady-state occupation probability $f(E)$ cannot be described by an effective temperature, its dependence on quasiparticle energy for $\Delta < E < 1.4\Delta$ is similar [33] to a thermal distribution with temperature of approximately 70 mK.

With $f(E)$ determined in this manner, we calculate the qubit excitation rate $\Gamma_\uparrow$ and decay rate $\Gamma_\downarrow$. For a tunnel junction with resistance R_T and capacitance C, and for normalized quasiparticle density of states $\rho(E) = E/\sqrt{E^2 - \Delta^2}$, the qubit decay rate induced by all quasiparticles is [13, 14]

$$\Gamma_\downarrow = \frac{1+\cos\phi}{R_T C}\int_\Delta^\infty \frac{dE}{E_{ge}}\frac{EE_f + \Delta^2}{EE_f}\rho(E)\rho(E_f)f(E), \tag{1}$$

where the final quasiparticle energy $E_f = E + E_{ge}$ is higher than E due to the absorption of the qubit energy E_{ge}. Here, ϕ is the junction phase, which is typically $\phi \simeq 0$ for the transmon and $\phi \simeq \pi/2$ for the phase qubit. For cold non-equilibrium quasiparticles, corresponding to $f(E)$ having population only at the gap energy Δ, this integral gives

$$\Gamma_\downarrow^c = \frac{1+\cos\phi}{\sqrt{2}\,R_T C}\left(\frac{\Delta}{E_{ge}}\right)^{3/2}\frac{n_{qp}}{n_{cp}}, \tag{2}$$

Here, $n_{cp} = D(E_F)\Delta$ is the Cooper pair density, $n_{qp} = 2D(E_F)\int_\Delta^\infty \rho(E)f(E)dE$ is the quasiparticle density, incorporating both hot and cold quasiparticles, and $D(E_F)/2$ is the single spin density of states. This is the standard result for quasiparticle dissipation [15], and is equivalent [14] to the Mattis-Bardeen theory [34] for $\phi = 0$.

In Fig. 2(a) we plot $\Gamma_\downarrow/\Gamma_\downarrow^c$, the ratio of the numerically-integrated qubit decay rate $\Gamma_\downarrow$ assuming both hot and cold non-equilibrium quasiparticles (Eq. 1) to the rate $\Gamma_\downarrow^c$ for cold quasiparticles at the gap (Eq. 2), with $f(E)$ calculated as explained above. We see that $\Gamma_\downarrow \approx \Gamma_\downarrow^c$ for a range of parameters, so the quasiparticle-induced decay rate is determined primarily by the total quasiparticle

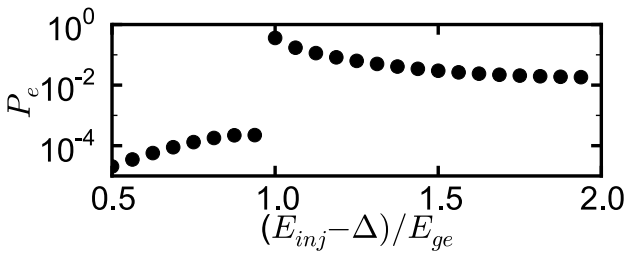

FIG. 3: Calculated qubit excitation probability P_e vs. quasiparticle injection energy E_{inj}. The injection energy is expressed as the fraction of the qubit energy $E_{ge} = h(6.7\,\mathrm{GHz})$ above the superconducting gap Δ. For $E_{inj} \gtrsim \Delta + 1.7E_{ge}$, P_e is essentially constant. Here, the injected quasiparticle density gives $n_{qp}/n_{cp} = 10^{-5}$.

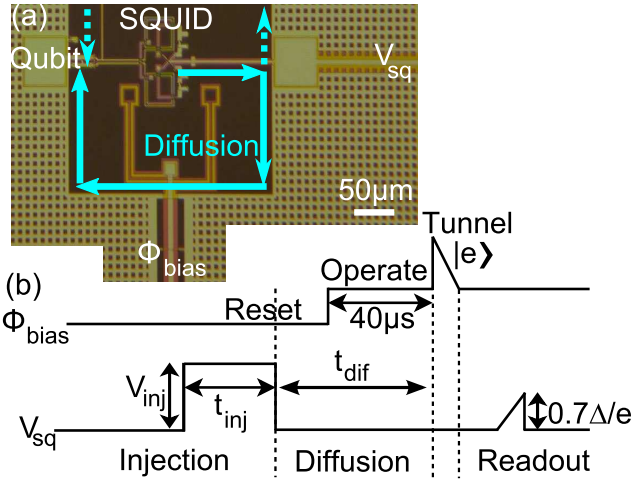

FIG. 4: (Color online) Experimental apparatus and protocol. (a) Photo of phase qubit, with voltage V_{sq} applied to the readout SQUID and flux bias Φ_{bias}. Two paths for quasiparticles to diffuse to the qubit junction are indicated by dotted and solid arrows. (b) Pulse sequence. Quasiparticles are generated with a voltage pulse on the SQUID line of amplitude $V_{inj} > 2(\Delta + E_{ge})/e$ for a time t_{inj}, which are varied to adjust the quasiparticle density. After a delay time t_{dif}, 40μs of which is at the operating bias, allowing quasiparticles to diffuse to the qubit, the qubit state is projected with a flux bias pulse and read out using a voltage pulse on the SQUID.

density n_{qp} and depends only weakly on the quasiparticle occupation distribution.

However, the quasiparticle distribution is key to characterizing the quasiparticle-induced steady-state excited state population, $P_e = \Gamma_\uparrow/(\Gamma_\downarrow + \Gamma_\uparrow)$. The rate $\Gamma_\uparrow$ can be evaluated using Eq. (1) by substituting $E_f = E - E_{ge}$, changing the lower limit of integration to $\Delta + E_{ge}$, and dropping the factor $(1 - f(E_f))$ as it has negligible effect. Using the same $f(E)$ as before, we calculate the probabilities plotted in Fig. 2(b). Notice that a non-negligible probability of a few percent can be obtained for quite modest quasiparticle densities. The probability P_e decreases for smaller quasiparticle densities and for larger qubit energies, as expected. For small occupation probabilities, this result can be approximated by the fit function $P_e \simeq 2.17(n_{qp}/n_{cp})(E_{ge}/\Delta)^{-3.65}$.

To determine the sensitivity of this result to the quasiparticle injection energy, we also calculated P_e as a function of the injection energy E_{inj}. As shown in Fig. 3, P_e is independent of the injection energy for $E_{inj} \gtrsim \Delta + 1.7E_{ge}$; hence, for sufficiently large injection energies, the actual injection value is unimportant. In addition, we see that P_e is significantly suppressed for quasiparticle energies below $\Delta + E_{ge}$, demonstrating that cold quasiparticles do not excite the qubit. The maximum at $E_{inj} = \Delta + E_{ge}$ is caused by the peaked final state density of states $\rho(E_f)$ at $E_f = \Delta$ in the expression for $\Gamma_\uparrow$.

To experimentally test these concepts, we performed an experiment in which we deliberately injected quasiparticles into a phase qubit and measured the excited state probability P_e and the increase in the qubit decay rate $\delta\Gamma_\downarrow$, which is proportional to n_{qp}/n_{cp} (Eq. 2). As shown in Fig. 4, we generated quasiparticles by applying a voltage pulse above the gap voltage Δ/e to the qubit's readout superconducting quantum interference device (SQUID), thus changing the quasiparticle density and $f(E)$. This is similar to previous work [14], except here the qubit measurements include the enhancement δP_e as a function of the energy relaxation rate increase $\delta\Gamma_\downarrow$. As shown in Fig. 4(b), we first applied a voltage pulse to the SQUID to generate above-gap quasiparticles; the duration t_{inj} of this pulse was varied to adjust the quasiparticle density. We reset the qubit into the $|g\rangle$ state using Φ_{bias} and then waited a variable time t_{dif} following the pulse, giving the quasiparticles time to diffuse to the qubit and allowing study of the temporal dynamics. After the qubit control pulses, we measured the qubit P_e, reading out the qubit by increasing V_{sq} to approximately $0.7\Delta/e$ to switch the SQUID into the normal state while minimizing quasiparticle generation.

In Fig. 5, we plot the observed changes δP_e versus $\delta\Gamma_\downarrow$ for two different phase qubits [6, 35] as we varied t_{dif} and t_{inj} over the ranges indicated in Table I. We find that δP_e monotonically increases with $\delta\Gamma_\downarrow$, thus scaling with quasiparticle density, as predicted by the theory. In fact, by deliberately injecting hot quasiparticles, we were able to increase P_e by more than 10%; this directly shows that hot quasiparticles can significantly excite the qubit.

The quasiparticle density was changed in three ways: Varying the diffusion time t_{dif} (triangles), the injection time t_{inj}, and the injection voltage V_{inj} (open vs. closed). There is essentially no difference between changing the injection voltage and the injection time; this makes sense, as P_e is relatively insensitive to the injection energy (Fig. 3). However, we observed a significant difference between varying the diffusion time and varying the injec-

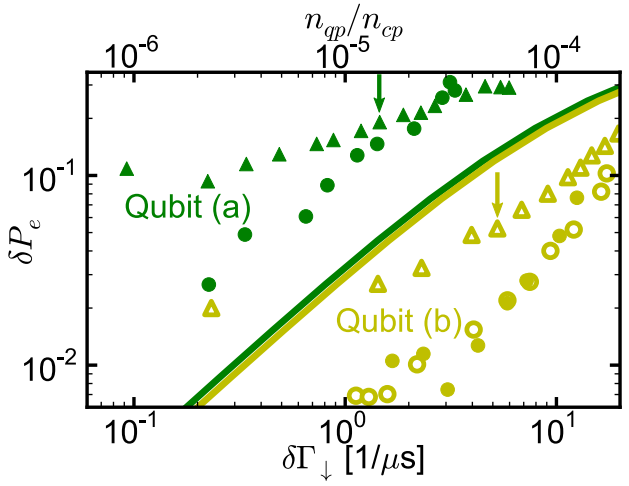

FIG. 5: (Color online) Experimental impacts of injected quasiparticles. Increases in qubit decay rate $\delta\Gamma_\downarrow$ (proportional to quasiparticle density n_{qp}/n_{cp}) and the raw qubit excited state probability δP_e are measured with respect to the values without quasiparticle injection. The quasiparticle density was parametrically varied by changing either the length t_{inj} of the injection pulse (circles) or the diffusion time t_{dif} (triangles); arrows indicate $t_{inj}+t_{dif}\sim 400\,\mu$s. Data are for two slightly different designs, as described by (a) [6] and (b) [35]; symbols and experimental parameters are defined in Table I. Theoretical predictions (solid lines) were calculated for quasiparticles injected at 1.9Δ using measured E_{ge}, giving $E_{ge}/\Delta\simeq 0.15$.

tion time. This is not surprising, as P_e is sensitive to the quasiparticle energy distribution, which changes with the diffusion time. As shown in Fig. 4a, quasiparticles generated at the measurement SQUID must diffuse through approximately 700 μm of ground plane metal in order to reach the qubit junction. This gives time for quasiparticle scattering and relaxation with respect to the injected distribution. In fact, those triangles in Fig. 5 where δP_e begins to level off correspond to $t_{inj}+t_{dif}\sim 400\,\mu$s (denoted by arrows). This is of the same order as typical quasiparticle recombination times [36, 37], where $f(E)$ is expected to become dominated by thermal equilibrium excitation independent of quasiparticle density. However, for times less than this (see Table I for times), the data where t_{dif} was varied is more similar to the data where t_{inj} is varied, indicating a non-thermal $f(E)$ dependence of P_e which varies with time.

Predictions from the model are plotted in Fig. 5 as solid lines. Although the power-law dependence (slopes) between model and measurement are in reasonable agreement, the model δP_e is low by about a factor of three for qubit (a) and high by about a factor of four for qubit (b). This can not be attributed to the small differences in the qubit geometries, because a third device (not shown), with the same design as (a), gave data about a factor of two lower than the model. These differences could be due to subtleties in the model not considered here. For

TABLE I: Parameters for data in Fig. 5. Here we list the parameter, t_{dif} or t_{inj}, that is varied for the five data sets, along with its values from the left to the right sides of the figure. The value of the fixed parameter and the injection voltage V_{inj} are also provided. Experimental parameters measured independently without quasiparticle injection include P_e, $\Gamma_\downarrow$, qubit frequency E_{ge}/h, and qubit critical current I_c.

Fig. 5 Symbols	Varied (μs)	Fixed (μs)	V_{inj} (Δ/e)	No Injection P_e	$1/\Gamma_\downarrow$	E_{ge}/h	I_c
(a) Closed Triangles	t_{dif} 540-68	t_{inj} 200	3.8	3.0%-3.7%	880 ns	5.8 GHz	1.0 μA
(a) Closed Circles	t_{inj} 8.4-200	t_{dif} 115	3.8	1%-9%	880 ns	5.5 GHz	1.0 μA
(b) Open Triangles	t_{dif} 740-90	t_{inj} 100	2.4	4.0%	380 ns	6.1 GHz	1.7 μA
(b) Open Circles	t_{inj} 5.0-50	t_{dif} 90	2.4	4.0%	380 ns	6.1 GHz	1.7 μA
(b) Closed Circles	t_{inj} 5.3-22	t_{dif} 140	3.4	4.7%	380 ns	6.1 GHz	1.7 μA

instance, there can be sample-to-sample variation such as a difference in film thickness or film quality, yielding variations in the gap energy, in the quasiparticle diffusion path, and in junction parameters. In addition, we note that the calculation of P_e assumes non-equilibrium quasiparticle relaxation through electron-phonon scattering and recombination. However, other effects such as quasiparticle diffusion and trapping of quasiparticles from non-uniform gaps may significantly affect the distribution $f(E)$, altering the prediction for the excitation rate. In addition, even though quasiparticles are expected to be generated with energies of $eV_{inj}/2$, in reality there will be a distribution of quasiparticle energies centered around this value for a given V_{inj}, so even for $eV_{inj}>2(\Delta+E_{ge})$, some of the generated quasiparticles may instead be cold. We conclude that the simple theoretical model used here for the quasiparticle energy distribution $f(E)$ is only semiquantitative, predicting $\Gamma_\uparrow$ in the non-thermal regime to about a factor of 4.

In conclusion, we have shown that "hot" quasiparticles with energies greater than $\Delta+E_{ge}$ can cause significant ground-to-excited state transitions in superconducting qubits. This is in contrast to "cold" quasiparticles solely at the gap, which only cause superconducting qubits to relax. This means quasiparticles cannot be adequately described by a single parameter such as n_{qp}/n_{cp} or temperature. As illustrated by varying both t_{inj} and t_{dif}, the particular quasiparticle distribution affects the observed qubit excitation probability. This theory semiquantitatively matches the observed behavior of the qubit excitation probability versus quasiparticle density.

Devices were made at the UC Santa Barbara Nanofab-

rication Facility, a part of the NSF-funded National Nanotechnology Infrastructure Network. This work was supported by IARPA under ARO award W911NF-09-1-0375. MM acknowledges support from an Elings Postdoctoral Fellowship. RB acknowledges support from the Rubicon program of the Netherlands Organisation for Scientific Research.

* Present address: Department of Physics, Zhejiang University, Hangzhou 310027, China
† Present address: IBM T.J. Watson Research Center, Yorktown Heights, NY 10598, USA
‡ Electronic address: martinis@physics.ucsb.edu

[1] J. Clarke and F. Wilhelm, Nature **453**, 1031 (2008).
[2] J.-S. Tsai, Proc. Jpn. Acad., Ser. B **86**, 275 (2010).
[3] M. Mariantoni *et al.*, Science **334**, 61 (2011).
[4] A. Fedorov, L. Steffen, M. Baur, M. P. da Silva, and A. Wallraff, Nature **481**, 170-172 (2012).
[5] M. D. Reed, L. DiCarlo, S. E. Nigg, L. Sun, L. Frunzio, S. M. Girvin, and R. J. Schoelkopf, Nature **482**, 382 (2012).
[6] E. Lucero *et al.*, Nature Phys., doi:10.1038/nphys2385, 2012 (to be published).
[7] J. Lisenfeld, C. Müller, J. H. Cole, P. Bushev, A. Lukashenko, A. Shnirman, and A. V. Ustinov, Phys. Rev. Lett. **105**, 230504 (2010).
[8] Y. Shalibo, Y. Rofe, D. Shwa, F. Zeides, M. Neeley, J. M. Martinis, and N. Katz, Phys. Rev. Lett. **105**, 177001 (2010).
[9] S. Gustavsson, J. Bylander, F. Yan, W. D. Oliver, F. Yoshihara, and Y. Nakamura, Phys. Rev. B **84**, 014525 (2011).
[10] D. Sank *et al.*, Phys. Rev. Lett. **109**, 067001 (2012).
[11] S. K. Choi, D.-H. Lee, S. G. Louie, and J. Clarke, Phys. Rev. Lett. **103**, 197001 (2009).
[12] G. Catelani, S. E. Nigg, S. M. Girvin, R. J. Schoelkopf, and L. I. Glazman, arXiv:1207.7084.
[13] J. M. Martinis, M. Ansmann, and J. Aumentado, Phys. Rev. Lett. **103**, 097002 (2009).
[14] M. Lenander *et al.*, Phys. Rev. B **84**, 024501 (2011).
[15] G. Catelani, J. Koch, L. Frunzio, R. J. Schoelkopf, M. H. Devoret, and L. I. Glazman, Phys. Rev. Lett. **106**, 077002 (2011).
[16] G. Catelani, R. J. Schoelkopf, M. H. Devoret, and L. I. Glazman, Phys. Rev. B **84**, 064517 (2011).
[17] L. Sun *et al.*, Phys. Rev. Lett. **108**, 230509 (2012).
[18] A. D. Córcoles, J. M. Chow, J. M. Gambetta, C. Rigetti, J. R. Rozen, G. A. Keefe, M. B. Rothwell, M. B. Ketchen, and M. Steffen, Appl. Phys. Lett. **99**, 181906 (2011).
[19] J. E. Johnson, C. Macklin, D. H. Slichter, R. Vijay, E. B. Weingarten, J. Clarke, and I. Siddiqi, Phys. Rev. Lett. **109**, 050506 (2012).
[20] K. Geerlings, S. Shankar, Z. Leghtas, M. Mirrahimi, L. Frunzio, R. J. Schoelkopf, and M. H. Devoret, in *Bulletin of the American Physical Society*, proceedings of the APS March Meeting, Boston, Massachusetts (American Physical Society, 2012), Z29.00009.
[21] A. Palacios-Laloy, F. Mallet, F. Nguyen, F. Ong, P. Bertet, D. Vion, and D. Esteve, Phys. Scripta **T137**, 014015 (2009).
[22] R. Barends *et al.*, Appl. Phys. Lett. **99**, 113507 (2011).
[23] D. Ristè, C. C. Bultink, K. W. Lehnert, and L. DiCarlo, arXiv:1207.2944.
[24] H. Paik *et al.*, Phys. Rev. Lett. **107**, 240501 (2011).
[25] J. Gao, J. Zmuidzinas, A. Vayonakis, P. Day, B. Mazin, and H. Leduc, J. Low Temp. Phys. **151**, 557 (2008).
[26] M. D. Reed, L. DiCarlo, B. R. Johnson, L. Sun, D. I. Schuster, L. Frunzio, and R. J. Schoelkopf, Phys. Rev. Lett. **105**, 173601 (2010).
[27] R. Vijay, D. H. Slichter, and I. Siddiqi, Phys. Rev. Lett. **106**, 110502 (2011).
[28] K. W. Murch, U. Vool, D. Zhou, S. J. Weber, S. M. Girvin, and I. Siddiqi, arXiv:1207.0053.
[29] F. Mallet, F. R. Ong, A. Palacios-Laloy, F. Nguyen, P. Bertet, D. Vion, and D. Esteve, Nature Phys. **5**, 791 (2009).
[30] K. Segall, C. Wilson, L. Li, L. Frunzio, S. Friedrich, M. C. Gaidis, and D. E. Prober, Phys. Rev. B **70**, 214520 (2004).
[31] S. B. Kaplan, C. C. Chi, D. N. Langenberg, J. J. Chang, S. Jafarey, and D. J. Scalapino, Phys. Rev. B **14**,4854 (1976).
[32] Equations (C3-C7) of [14] are used to calculate the quasiparticle number distribution for a given injection rate. The quasiparticle energy distribution $f(E)$ is then calculated using Eq. (C1), and the total quasiparticle density is calculated with Eq. (C2).
[33] This is determined from the nearly-constant slope in the region $1 < E/\Delta < 1.4$ of Fig. 1 in [13] given $n_{qp}/n_{cp} = 1.8 \times 10^{-6}$ (calculated using [32]).
[34] D. Mattis and J. Bardeen, Phys. Rev. **111**, 412 (1958).
[35] Y. Yin *et al.*, arXiv:1208.2950.
[36] R. Barends, J. J. A. Baselmans, S. J. C. Yates, J. R. Gao, J. N. Hovenier, and T. M. Klapwijk, Phys. Rev. Lett. **100**, 257002 (2008).
[37] B. A. Mazin, D. Sank, S. McHugh, E. A. Lucero, A. Merrill, J. Gao, D. Pappas, D. Moore, and J. Zmuidzinas, Appl. Phys. Lett. **96**, 102504 (2010).